www.czasopisma.pan.pl PAN POLSKA AKADEMIA NAUK www.journals.pan.pl

Arch. Metall. Mater. **65** (2020), 2, 827-837

DOI: 10.24425/amm.2020.132828

D. BOCHENEK[1], P. NIEMIEC[1*], E. ĆWIKIEL[1], T. GORYCZKA[1]

# PZT-TYPE CERAMICS DOPED WITH MANGANESE, ANTIMONY, LANTHANUM AND TUNGSTEN – TECHNOLOGY AND PHYSICAL PROPERTIES

The work three ceramic compositions based on $PbZr_{0.49}Ti_{0.51}O_3$ doped with manganese (Mn), antimony (Sb), lanthanum (La) and tungsten (W) were obtained. The introduction of a set of admixtures was aimed at improving the sinterability of ceramic materials and optimizing its electrophysical parameters. Multi-component materials of the PZT-type with a general formula: $Pb(Zr_{0.49}Ti_{0.51})_{0.94}Mn_{0.021}Sb_{0.016}La_yW_zO_3$ (where $y$ from 0.008 to 0.012 and $z$ from 0.012 to 0.014) were prepared by the conventional mixed oxide method. After mixing and drying the powder mixtures were calcined in air at 850°C for 4 h, while densification of the powders was carried out by the free sintering method at 1150°C for 2 h. The final steps of technology were grinding, polishing, annealing and putting silver paste electrodes onto both surfaces of the samples for electrical testing.

XRD, SEM, EDS, dielectric, ferroelectric, piezoelectric properties and DC electrical conductivity of the obtained ceramic compositions were carried out. X-ray tests of the crystal structure conducted at room temperature have shown that all obtained the PZT-type materials were a single phase (perovskite type) without the presence of a foreign phase. Symmetry of the crystal lattice was identified as space group P4mm. Temperature dielectric studies have shown high values of dielectric permittivity and low dielectric loss. The presented physical properties of ceramic samples based on PZT confirm their predisposition for application in modern microelectronic and micromechatronic applications.

*Keywords:* PZT-type ceramics, perovskite type materials, ferroelectrics; doped

## 1. Introduction

The necessary requirements for ceramic materials with functional properties in modern microelectronics are their high and stable performance parameters. A doped piezoceramics based on PZT ($PbZr_{1-x}Ti_xO_3$, where $x$ from 0 to 1.0) belongs to ferroelectric materials with versatile and optimal properties in piezoelectric applications [1-6].

These materials exhibit a domain structure and spontaneous polarization at temperatures below the Curie point. The phase diagram of the solid solution $PbZr_{1-x}Ti_xO_3$ created in the 1960s by Jaffe [7] presents the ranges of occurrence in this material of various phases of the crystalline structure, which give these materials various properties. Depending on the Zr/Ti ratio ($x$), the PZT solid solution has an antiferroelectric rhombic structure (for $0 < x < 0.042$), a rhombohedral structure (for $0.042 < x < 0.38$ – R3c and $0.38 < x < 0.47$ – R3m), tetragonal structure (for $0.48 < x < 1.0$) or crystallized in a morphotropic area ($0.47 < x < 0.48$), in which a mixture of rhombohedral and tetragonal phases [7-10] occurs. In this area there are extremely high or extremely low physical properties of the material. The introduction of appropriate admixtures to the basic composition of PZT significantly improves the final properties of ceramics, and the morphotropic area is shifted and / or widened [11-13].

Based on many years of practice, ceramic materials based on the PZT (three, four, five and more admixture components) are currently being developed due to the significant improvement in physical properties, as well as a further extension of the functional applicability of such materials.

In order to search for newer applications based on the PZT materials, ceramic composites [14-18], ceramic-polymer [19-20] and also thin layers [21] are also designed and obtained. Piezoceramic based on PZT is widely used for examples: stacked actuators for atomic force microscopy and nanopositioners, high speed valves for fuel injection, vibration control devices, depth finders and hydrophones, and linear and rotary piezomotors, tube actuators (comprise the active mechanisms in micropumps and

[1] UNIVERSITY OF SILESIA IN KATOWICE, FACULTY OF SCIENCE AND TECHNOLOGY, INSTITUTE OF MATERIALS ENGINEERING, 75 PUŁKU PIECHOTY 1A, 41-500 CHORZÓW, POLAND

* Corresponding author: przemyslaw.niemiec@us.edu.pl

scanning and atomic force microscopes), bender-type transducers, such as the unimorph and bimorph designs (are employed in pneumatic values, high speed camera shutters, energy harvesting devices, piezoelectric transformers, and inkjet printers), bending-type PZT actuators (are employed in ultrasonic transducers for dental tools and biomedical imaging and treatment), sensors (include accelerometers, knock sensors to monitor engine combustion, pressure and force sensors, ultrasonic distance sensors, and vibration sensors to monitor automotive, railroad, and aircraft components and in high voltage spark igniters), energy harvesting devices [22-31].

In the paper three compositions based on PZT ceramics (Zr/Ti = 0.49/0.51) doped with manganese (Mn), antimony (Sb), lanthanum (La) and tungsten (W) were obtained for application in modern microelectronics and micromechatronics. In the above compositions a variable amount of lanthanum (from 0.008 to 0.012) and tungsten (from 0.014 to 0.012) admixture were used.

## 2. Experiment

Multi-component materials of the PZT-type with a general formula: $Pb(Zr_{0.49}Ti_{0.51})_{0.94}Mn_{0.021}Sb_{0.016}La_yW_zO_3$ (where $y$ from 0.008 to 0.012 and $z$ from 0.012 to 0.014) were prepared by the conventional mixed oxide method. The starting oxides PbO (99.99%, POCH), $ZrO_2$ (99.00%, Merck), $TiO_2$ (99.99%, Merck), $MnO_2$ (99%, Aldrich), $Sb_2O_3$ (99.995%, Aldrich), $La_2O_3$ (99.5%, Aldrich), and $WO_3$ (99.9%, Fluka) were milled in the planetary mill FRITSCH Pulwerisette 6 for 24 h in ethanol using zirconium balls using. An additional 5 wt.% PbO was added to compensate for PbO evaporation during technological process. After mixing and drying the powder mixtures were calcined in air at 850°C for 4 h (at heating rate of 150°C/h). Densification of the synthesized powders was carried out by the free sintering method at 1150°C for 2 h (heating rate of 150°C/h). The final steps of technological process were grinding, polishing, removing mechanical stresses (annealing at temperature 700°C/15 min.) and putting silver paste electrodes onto both surfaces of the samples for electrical testing. The process was made by firing silver paste in the following conditions: 850°C/15 min.

Three materials of the PZT-type were obtained with the following chemical compositions: materials with a general formula:

(i) $Pb(Zr_{0.49}Ti_{0.51})_{0.94}Mn_{0.021}Sb_{0.016}La_{0.012}W_{0.012}O_3$ (s-La12);

(ii) $Pb(Zr_{0.49}Ti_{0.51})_{0.94}Mn_{0.021}Sb_{0.016}La_{0.010}W_{0.013}O_3$ (s-La10);

(iii) $Pb(Zr_{0.49}Ti_{0.51})_{0.94}Mn_{0.021}Sb_{0.016}La_{0.008}W_{0.014}O_3$ (s-La08).

X-ray testes of the crystal structure were conducted at room temperature using X'Pert-Pro PW3040/60 diffractometer (PANalytical, Eindhoven, The Netherlands). The X-ray diffraction patterns were stored at range of 2q from 10° to 100° in step-scan mode: 0.05 degrees and 4 s/step and the copper radiations $CuK_{\alpha1}/_{\alpha2}$ (wavelength 0.154045 nm/ 0.15444 nm), were used. EDS (Energy Dispersive Spectrometry), EPMA (Electron Probe Micro Analyzer) and the SEM microstructure of fracture of the samples were carried out by a scanning electron microscopy JSM-7100F TTL LV (Jeol Ltd., Tokyo, Japan). The samples were coated with gold to provide electrical conductivity in order to obtain charging effects. Temperature dielectric measurements (dielectric permittivity and dielectric loss) were made on the capacity bridge LCR Meter (Quad Tech 1929 Precision LCR Meter, Quad Tech, Inc. Maynard, MA, USA), at temperature range of 20°C to 450°C (a heating cycle, a heating rate of 1.0 deg./min., frequency range of 1 kHz to 100 kHz). Temperature measurements of DC electric conductivity were conducted using a Keithley 6517B electrometer (Keithley Instruments, Cleveland, OH, USA), in the temperature range of 20°C to 450°C (a heating cycle). Hysteresis ($P$–$E$) loops were performed using a Sawyer-Tower circuit and a high voltage amplifier (HEOPS-5B6 precision, Matsusada Precision Inc., Kusatsu, Japan) at room temperature and for the frequency of the measurement field from the interval 100 mHz-100 Hz. The data were stored on a computer disc using an A/D, D/A transducer card (National Instruments Corporation, Austin, TX, USA) and the LabView computer program.

In order to test piezoelectric parameters the PZT-type ceramic samples were polarized by a high voltage method using a high voltage amplifier (HEOPS-5B6 precision, Matsusada Precision Inc., Kusatsu, Japan). For all ceramic samples poling process was performed in a silicone oil in the following conditions: poling field $E_{pol} = 2.0$ kV/mm, poling time $t_{pol} = 0.5$ h and at poling temperature $T_{pol} = 150$°C. Cooling the ceramic sample to room temperature was carried out at an applied electric field. Examinations of the piezoelectric parameters were carried out using the resonance–antiresonance method. The piezoelectric coefficient $d_{33}$ was measured at room temperature using a YE2730A d33 meter (APC International Ltd., Mackeyville, PA, USA).

## 3. Results and discussion

Fig. 1 shows comparison of the X-ray diffraction patterns measured at room temperature for the PZT-type ceramics. All X-diffraction lines, presented in the patterns, were identified as a one belonging to the perovskite type of structure with tetragonal crystal lattice.

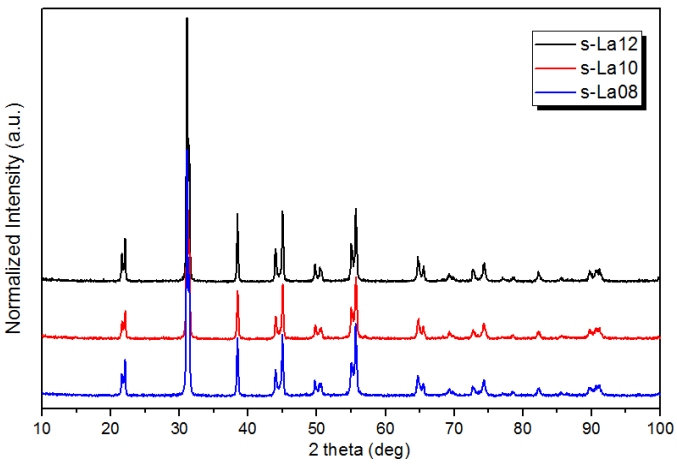


Fig. 1. X-ray diffraction patterns of the PZT-type ceramics

All ceramic samples were a single phase without the presence of a foreign phases (no other or impurity phase peaks are seen in the XRD data). In order to determine the lattice parameters, the X-ray diffraction patterns were fitted using the Rietveld method [32]. Symmetry of the crystal lattice can be described using space group P*4mm*. Results of determined lattice parameters were shown in Table 1. A change in the amount of lanthanum in the base $Pb(Zr_{0.49}Ti_{0.51})_{0.94}Mn_{0.021}Sb_{0.016}La_zW_{0.014}O_3$ composition causes a slight change in the value of the parameter $c$ and the volume of the elementary cell $V$, but without a clear tendency.

Based on diffraction studies, it was determined minimal possible size of crystals, the dislocation density and the microstrain of the PZT-type ceramic samples. A minimal possible size of crystals of the ceramic samples was estimate from the Full Width at Half Maximum (FWHM) of the strongest X-ray diffraction peak (110) according Scherrer equation (1):

$$D = \frac{0.9\lambda}{\beta\cos\theta} \tag{1}$$

where: $D$ is the particle diameter, $K$ is dimensionless shape factor (shape factor has a typical value of about 0.9), l is the X-ray wavelength, b is FWHM of the main diffraction peak (110), q is a Bragg angle [33]. The Scherrer method uses the relationship between the size of crystallites and the broadening of the profile of diffraction lines. The smaller the grain sizes in the material, the greater the reflex widening. The calculated size of crystallites $D$ was in the range of 29.66 nm – 35.54 nm (i.e. 35.54 nm, 29.66 nm and 32.98 nm, for s-La12, s-La10 and s-La08 samples, respectively).

The dislocation density $\delta$ (the amount of defects in a crystal defined as the length of dislocation lines per unit volume) was estimated according the following formula [34]:

$$\delta = \frac{1}{D^2} \tag{2}$$

The microstrain $\xi$ (structural parameter) was calculated from the equation [35]:

$$\xi = \frac{\beta}{4\tan\theta} \tag{3}$$

The minimal possible size of crystals $D$, the dislocation density $\delta$ and the microstrain $\xi$ of the ceramic samples are summarized in Table 1.

Microstructural SEM images of PZT ceramic compositions are depicted in Fig. 2 (Fig. 2a,c,e for 2k magnification and Fig. 2b,d,f for 5k magnification). The microstructure SEM images of all the samples are characterized by densely packed grains with properly crystallized grain (the grains are well grown). The samples present compact structure, whereas ceramic grains have expressive and sharp grain boundaries. This proves that the sintering parameters have been correctly selected and that the entire technological process of the ceramic samples has been correctly carried out.

The obtained multi-component materials are characterized by high density with low porosity. On the fracture of the samples a distinct cracking is observed both on the grain boundary (in a significant advantage) and through the grain itself. In all compositions, it can be observed that the mechanical strength of both the grain boundaries and the grain itself is equally high.

Cracking through grain does not cause breakdown into small ceramic elements, but the structure inside the grain is solid, with a strong consolidated structure (Fig. 2b, 2d). Comparing the microstructures of the analyzed compositions of the PZT ceramics, it can be concluded that the largest and the smallest

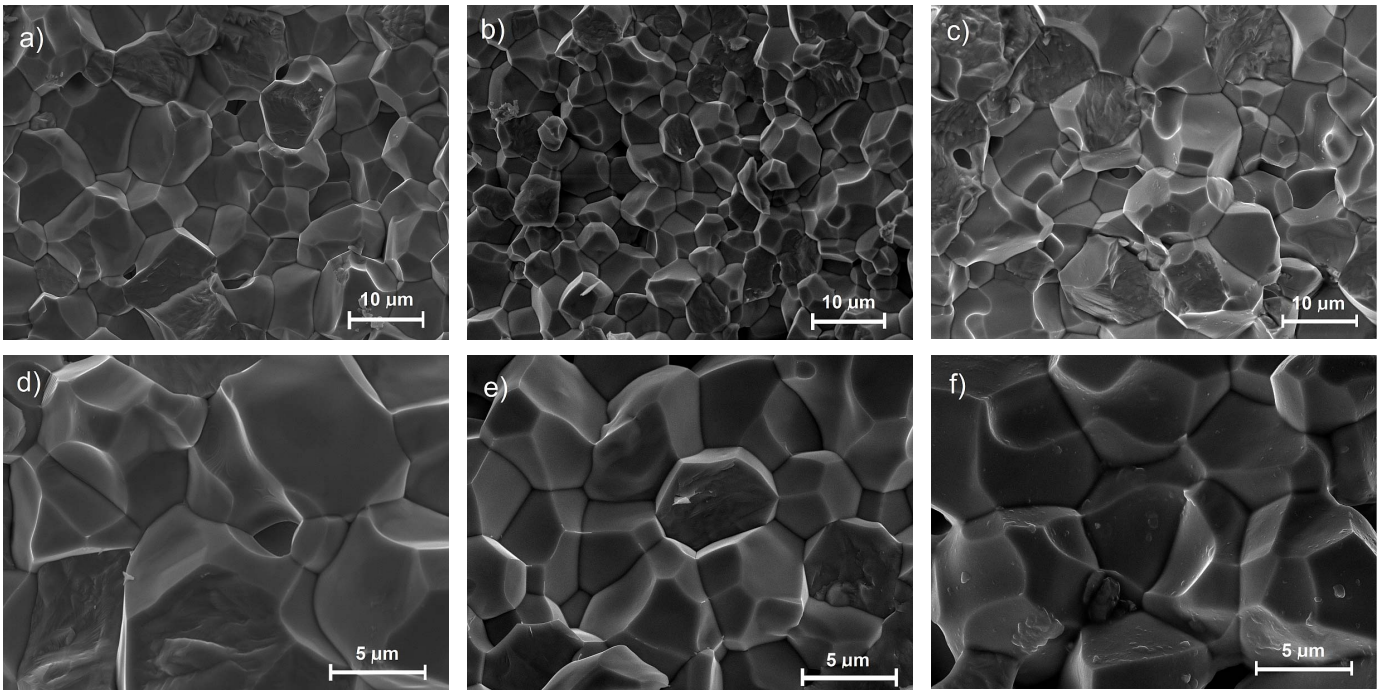


Fig. 2. SEM images of the microstructure of PZT-type specimen fractures: a), d) s-La12, b), e) s-La10, c), f) s-La08 (magnification × 2k, × 5k, respectively)

TABLE 1

Parameters of the PZT-type samples

| | **s-La12** | **s-La10** | **s-La08** |
|---|---|---|---|
| $a_0$ (Å) | 4.0323 | 4.0314 | 4.0350 |
| $b_0$ (Å) | 4.0323 | 4.0314 | 4.0350 |
| $c_0$ (Å) | 4.1205 | 4.1154 | 4.1217 |
| $V_0$ (Å$^3$) | 67.0 | 66.9 | 67.1 |
| $D$ (nm) | 35.54 | 29.66 | 32.98 |
| $\delta \times 10^{-4}$ | 7.92 | 11.37 | 9.19 |
| $\xi$ | 0.207 | 0.251 | 0.225 |
| $\rho_{DC}$ at $RT$ (Wm) | $1.98\times10^{8}$ | $1.50\times10^{8}$ | $1.40\times10^{11}$ |
| $E_a$ in I (V) | 0.551 | 0.562 | 0.563 |
| $E_a$ in II (eV) | 0.875 | 0.859 | 0.804 |
| $T_C$ (°C)[1] | 295 | 298 | 292 |
| $\varepsilon_r$ at $RT$[1] | 1054 | 1034 | 921 |
| $\varepsilon_{max}$ at $T_C$[1] | 20230 | 17800 | 17175 |
| tand at $RT$[1] | 0.0042 | 0.0053 | 0.0060 |
| $P_S$ (mC/cm$^2$) at $RT$ | 10.04 | 9.97 | 11.46 |
| $P_r$ (mC/cm$^2$) at $RT$ | 6.27 | 6.15 | 7.28 |
| $E_c$ (kV/mm) at $RT$ | 0.915 | 1.01 | 0.967 |
| $d_{33}$ (pC/N) at $RT$ | 336 | 330 | 324 |
| $k_p$ | 0.54 | 0.52 | 0.47 |
| $d_{31}$ (pC/N) | 125.11 | 122.63 | 107.12 |
| $g_{31} \times 10^3$ [Vm/N] | 9.93 | 11.5 | 10.2 |
| $V_r$ (m/s) | 2022 | 1987 | 1940 |

[1] for $\nu$ = 1 kHz, $RT$ – room temperature

amounts of lanthanum additive (s-La12 and s-La08 samples) cause an increase in the average grain size. The grain growth is also accompanied by an increase in grain size heterogeneity. Large ceramic grains grow at the expense of small grains, which results in increased uneven grain growth across the microstructure of the ceramic samples. In the case of s-La10 sample, in which the amounts of lanthanum admixture have intermediate values, on the microstructural SEM images a reduction in the average grain size is observed, and the homogeneity of the grains in the whole sample volume is increased.

Examples of EPMA (Electron Probe Micro Analyzer) test results for the $Pb(Zr_{0.49}Ti_{0.51})_{0.94}Mn_{0.021}Sb_{0.016}La_yW_zO_3$ ceramic samples are displayed in Fig. 3. For the EPMA maps, the distribution in the sample volume of the admixtures used (manganese (Mn), antimony (Sb), lanthanum (La) and tungsten (W)) were made. The EPMA tests of the obtained samples show that the applied admixtures introduced into the base composition are distributed uniformly throughout the entire sample volume.

Fig. 4 presents the results of EDS tests of the ceramic samples together with an example SEM photo of the analyzed surface. The EDS analysis was carried out on 10 freely selected measurement areas, and the results were averaged.

In the case of basic compounds of PZT material, for all tested compositions, EDS analysis showed a slight excess of lead and a slight underflow of zirconium, while the content of titanium is very close to the theoretical amount (Table 2). In the case of admixtures: the amount of lanthanum remains at the assumed level, while the remaining admixtures of manganese, antimony and tungsten show a slight deficiency. However, the conducted analysis confirmed that for all materials there are slight deviations from the assumed chemical composition, and these deviations remain within the normal range.

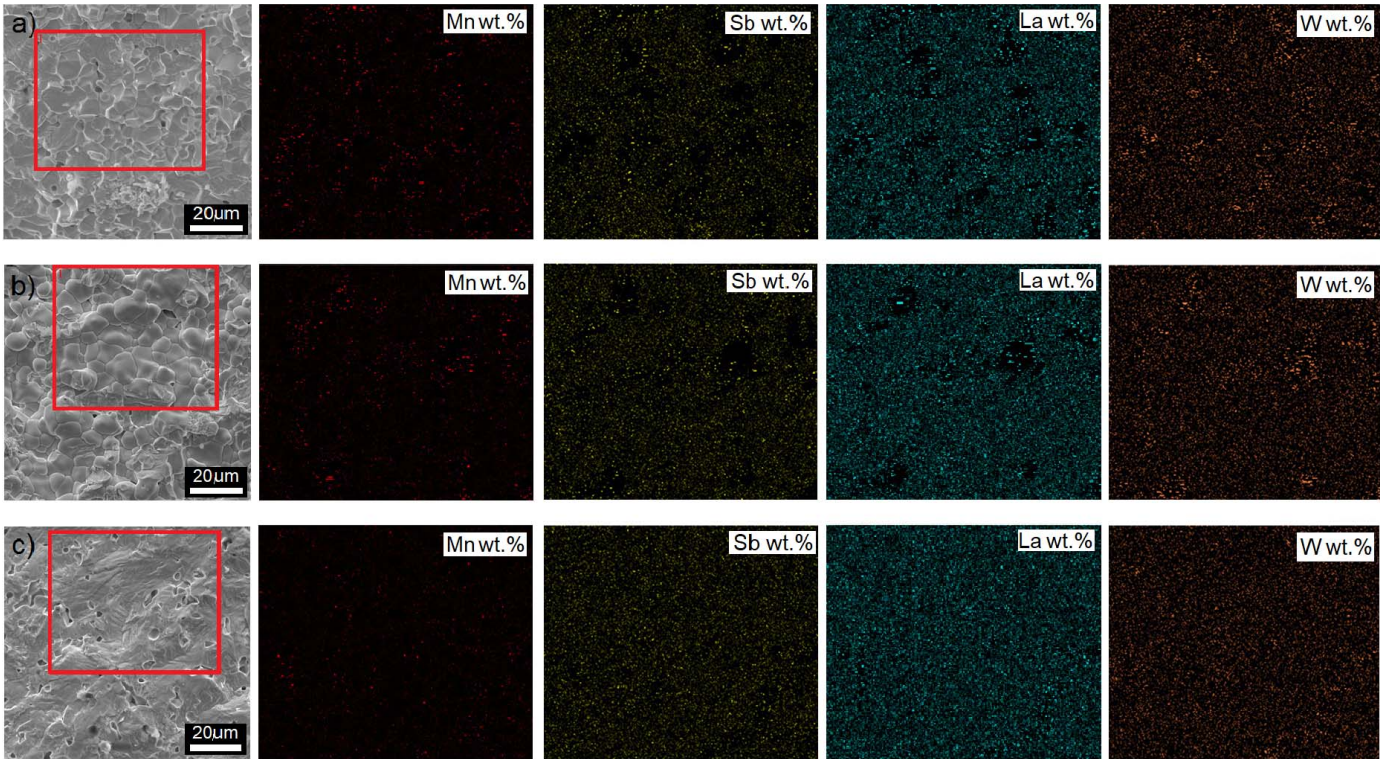


Fig. 3. EPMA test results for the PZT-type ceramics a) s-La12, b) s-La10, c) s-La08

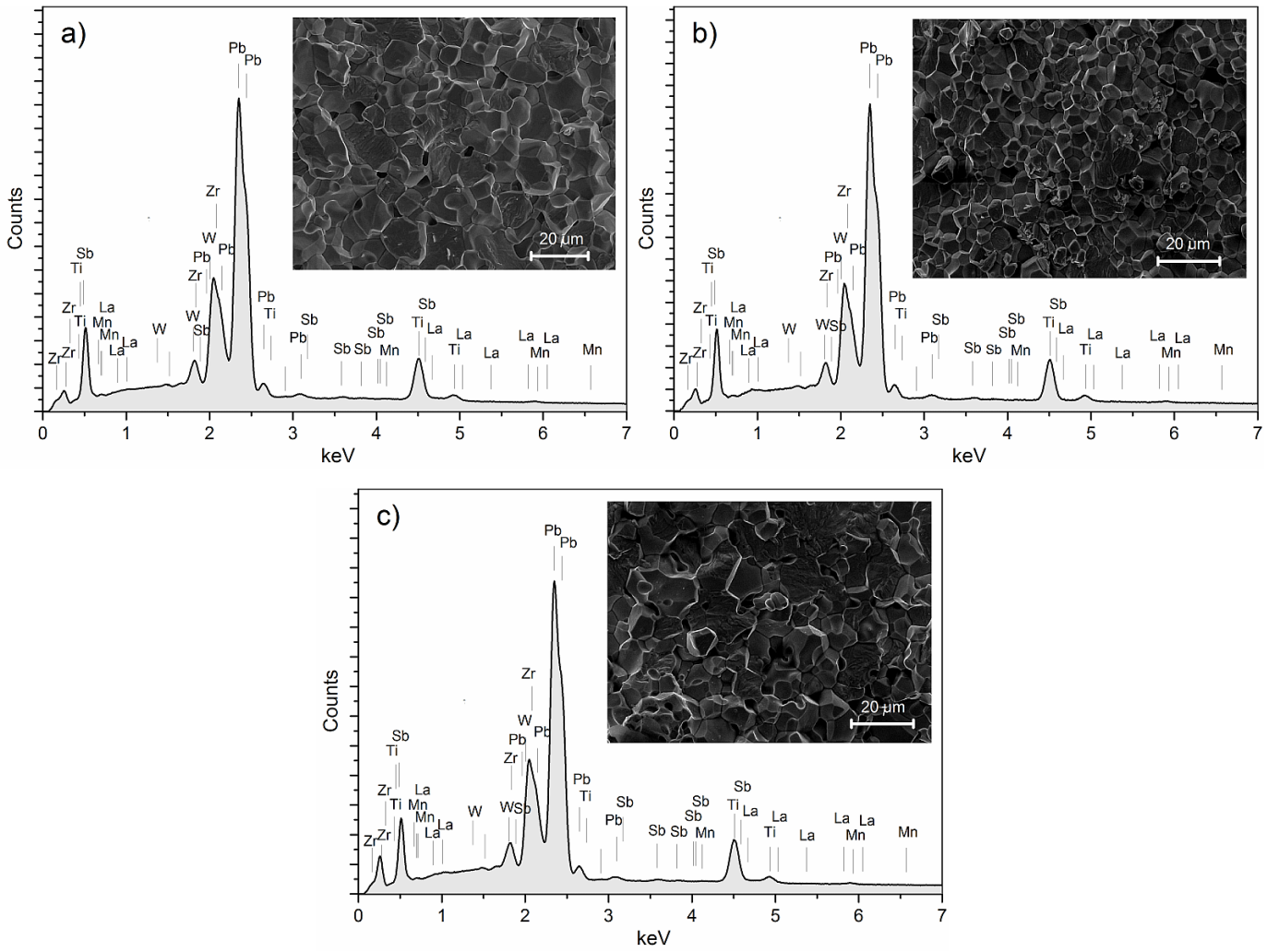


Fig. 4. The EDS analysis image of the element distribution for the PZT-type ceramics: a) s-La12, b) s-La10, c) s-La08

TABLE 2

Theoretical and experimental percentages of elements of PZT-type ceramics.

| | s-La12 | | s-La10 | | s-La08 | |
|---|---|---|---|---|---|---|
| | **Theoret. (%)** | **Exper. (%)** | **Theoret. (%)** | **Exper. (%)** | **Theoret. (%)** | **Exper. (%)** |
| PbO | 68.22 | 69.77 | 68.24 | 69.65 | 68.26 | 69.66 |
| $ZrO_2$ | 17.35 | 16.29 | 17.35 | 16.35 | 17.36 | 16.28 |
| $TiO_2$ | 11.71 | 11.69 | 11.71 | 11.73 | 11.71 | 11.72 |
| $MnO_2$ | 0.56 | 0.45 | 0.56 | 0.42 | 0.56 | 0.46 |
| $Sb_2O_3$ | 0.71 | 0.61 | 0.71 | 0.62 | 0.71 | 0.60 |
| $La_2O_3$ | 0.60 | 0.60 | 0.50 | 0.50 | 0.40 | 0.39 |
| $WO_3$ | 0.85 | 0.59 | 0.92 | 0.73 | 0.99 | 0.89 |

In microelectronic devices a ferroelectric materials are often subjected to high electric loads (stress), causing nonlinear dielectric and piezoelectric response of ceramic samples [36]. Dielectric responses are dependent on both intrinsic and extrinsic mechanisms. The intrinsic contribution relates to the lattice (elementary cell), and is the average response of individual ferroelectric domains in the ceramic materials. The extrinsic contributions are the result of existence of the domain walls, the phase boundaries, and the defect dipoles [36]. So, the domain structure of a ferroelectric ceramic materials has a great influence on their dielectric properties. Temperature dependences of dielectric permittivity made for frequencies from 1 kHz to 100 kHz are shown in Fig. 5. All designed compositions of the PZT-based materials show very high values of dielectric permittivity with a clear, sharp phase change. This proves that the technological process has been properly carried out with the susceptible selection of sintering process conditions. The increase in the frequency of the measurement field results in the reduction of the dielectric permittivity value, without the shift of the phase change temperature (so-called frequency dispersion), which is characteristic for the relaxation materials.

A character of the phase transition diffusion of the perovskite materials shows a degree of the crystalline structure ordering. When ordering is greater a phase transition taking place in a narrow temperature range is observed. Acute phase transition from ferroelectric to paraelectric phase positive influence on the utility parameters of that kind of the ceramic materials [37]. The temperature dependence of the dielectric permittivity ($\varepsilon$) far from temperature $T_m$ is well described by the linear Curie-Weiss law. Near $T_m$ temperature dependence $\varepsilon(T)$ is approximated by

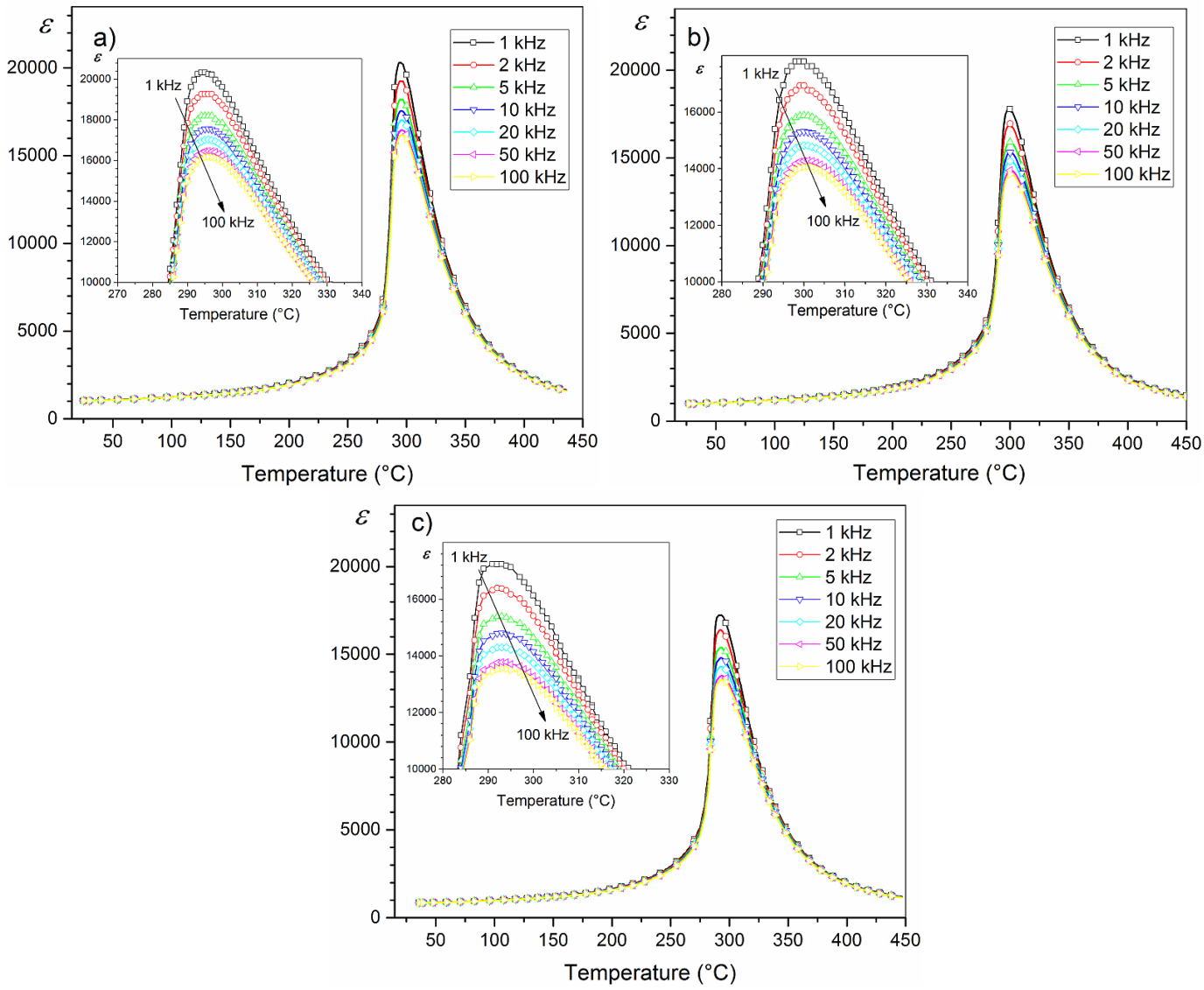


Fig. 5. The $\varepsilon(T)$ temperature relationships for the PZT-type ceramics: a) s-La12, b) s-La10, c) s-La08 (a heating cycle)

the quadratic Curie-Weiss law [36]:

$$\frac{1}{\varepsilon}-\frac{1}{\varepsilon_m}=C\left(T-T_m\right)^{\alpha} \tag{4}$$

where $T_m$ is the temperature at which dielectric permittivity is the largest ($\varepsilon_m$), $C$ is a temperature independent function, $\alpha$ is an exponent showing a diffusion degree of the phase transition (from the ferroelectric to paraelectric one). Where the $\alpha$ parameter is equal 1 indicates normal Curie-Weiss behavior, while if $1<\alpha\leq 2$ then the phase transition has a diffusive character [36]. A character and a degree of the phase transition diffusion can be also specified as a ratio of the maximum dielectric permittivity and the dielectric permittivity at room temperature ($\varepsilon_m/\varepsilon_r$). The dielectric parameters, for frequency $\nu = 1$ kHz are presented in Table 1.

The temperature waveforms of dielectric loss for the obtained samples tested for the field frequency from 1 kHz to 100 kHz are depicted in Fig. 6. Increasing the field frequency reduces the value of dielectric loss. All tested compositions are characterized by low values of dielectric loss, with the local maximum (peak occurring just before the phase transition) characteristic for PZT materials. A further increase in temperature causes a decrease in the dielectric loss, while above 350°C the values of dielectric loss grow rapidly (increase of electrical conductivity at high temperatures).

Fig. 7 presents the summary of dielectric properties of the PZT-type ceramic samples 1 kHz in the temprature range of 20 to 450°C (Fig. 7a dielectric permittivity and Fig. 7b dielectric loss). The comparative comparison of the graphs showed that all samples have equally high values of dielectrical permittivity as well all very low dielectric loss.

The frequency dependences of dielectric permittivity at various temperatures (from 25°C to 400°C) of the PZT-type ceramics are shown in Fig. 8. Below the phase change temperature values of dielectric permittivity decreases with the increase of frequency (in frequency region from 20 Hz to 10 kHz), and next attains a constant value at higher frequencies. This is typical for Debeye-like relaxation.

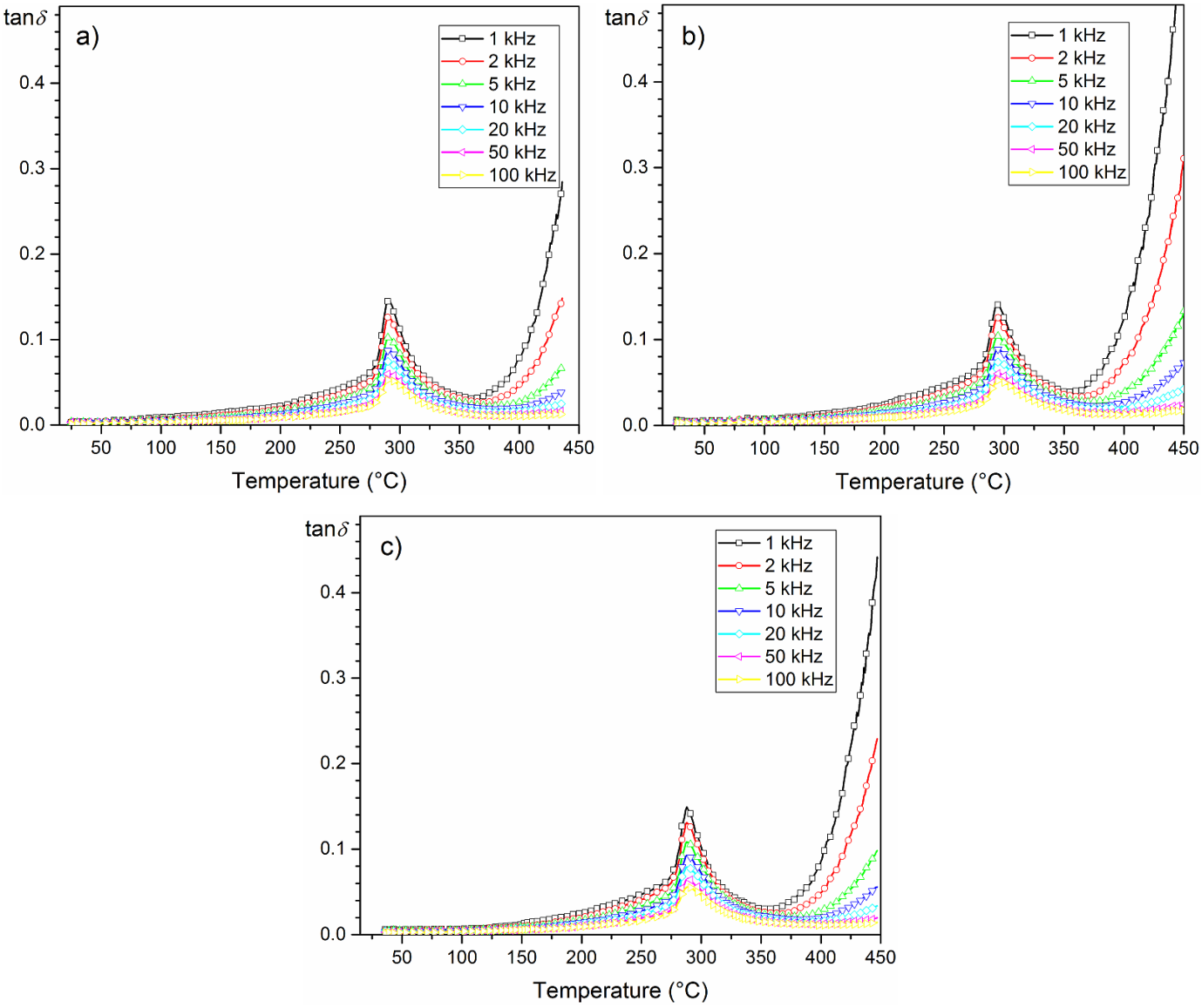


Fig. 6. Temperature dependences of the tan$\delta$ for the PZT-type ceramics: a) s-La12, b) s-La10, c) s-La08 (a heating cycle)

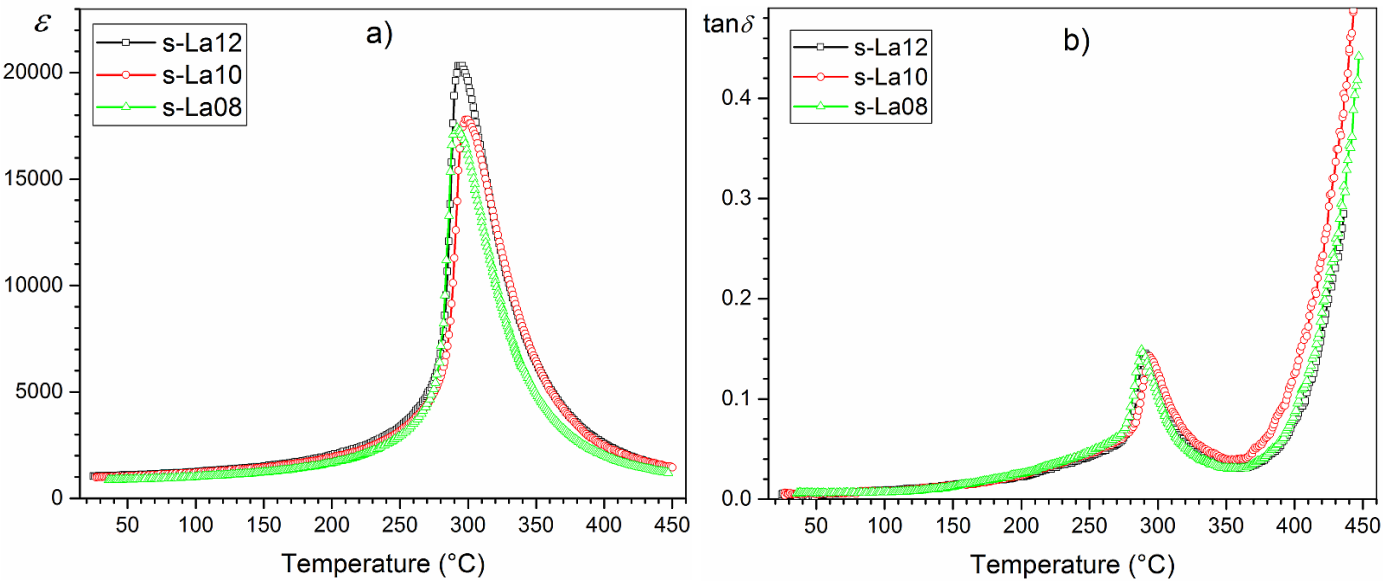


Fig. 7. Summary of the results of the dielectric properties for the PZT-type material (for 1 kHz), a) $\varepsilon(T)$ and b) tan$\delta(T)$

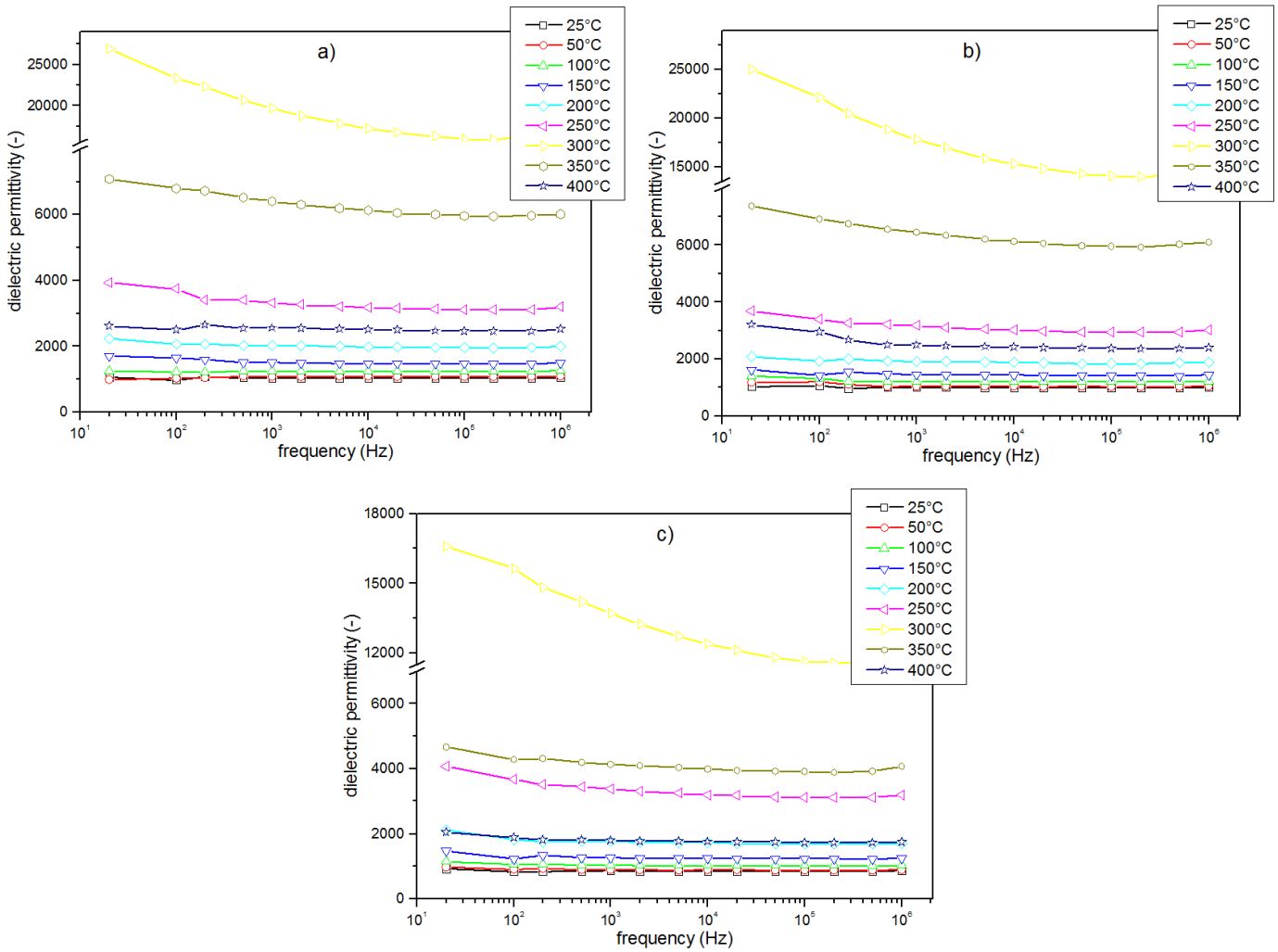


Fig. 8. Frequency dependences of dielectric permittivity of the PZT-type material: a) s-La12, b) s-La10, c) s-La08

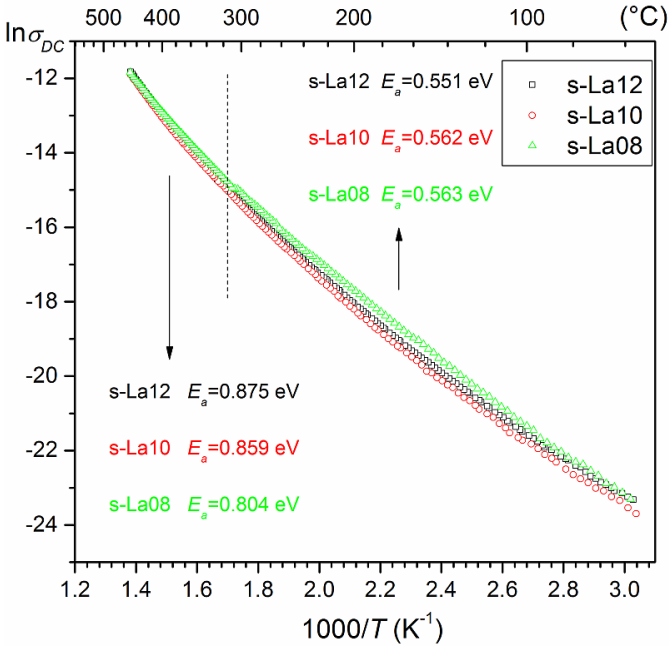


Fig. 9. The ln$\sigma_{DC}$(1000/$T$) dependences of the PZT-type material

The temperature dependencies of ln$\sigma_{DC}$(1000/$T$) for all compositions of the PZT-type material is depicted in Fig. 9. All compositions obtained show similar waveforms of temperature dependence of electrical conductivity. As the temperature rises, a slow increase in electrical conductivity in the materials is observed. A slight change in the amount of lanthanum (in the range from 0.008 to 0.012) at the expense of the amount of tungsten (in the range from 0.012 to 0.014) does not change the nature of the electrical conductivity in the measured ceramics. In the PZT-type materials donor dopants (like $La^{3+}$, $W^{6+}$), create metal (cation) vacancies and facilitate domain wall motion in the ceramic materials (donor doping creates soft PZT, while acceptor doping creates hard PZT) [38].

Below the phase transition temperature, the $E_a$ activation energy values are lower than for the temperature interval above the phase transition. This is a characteristic feature of PZT-type ceramic materials with a perovskite-like structure. For the tested compositions (in appropriate temperature ranges) also the $E_a$ activation energies have similar values (Fig. 9).

One with feature of the ferroelectric behavior of a material is the polarization-electric field ($P$-$E$) hysteresis loop. The polarization of a ferroelectric materials is the summation of total

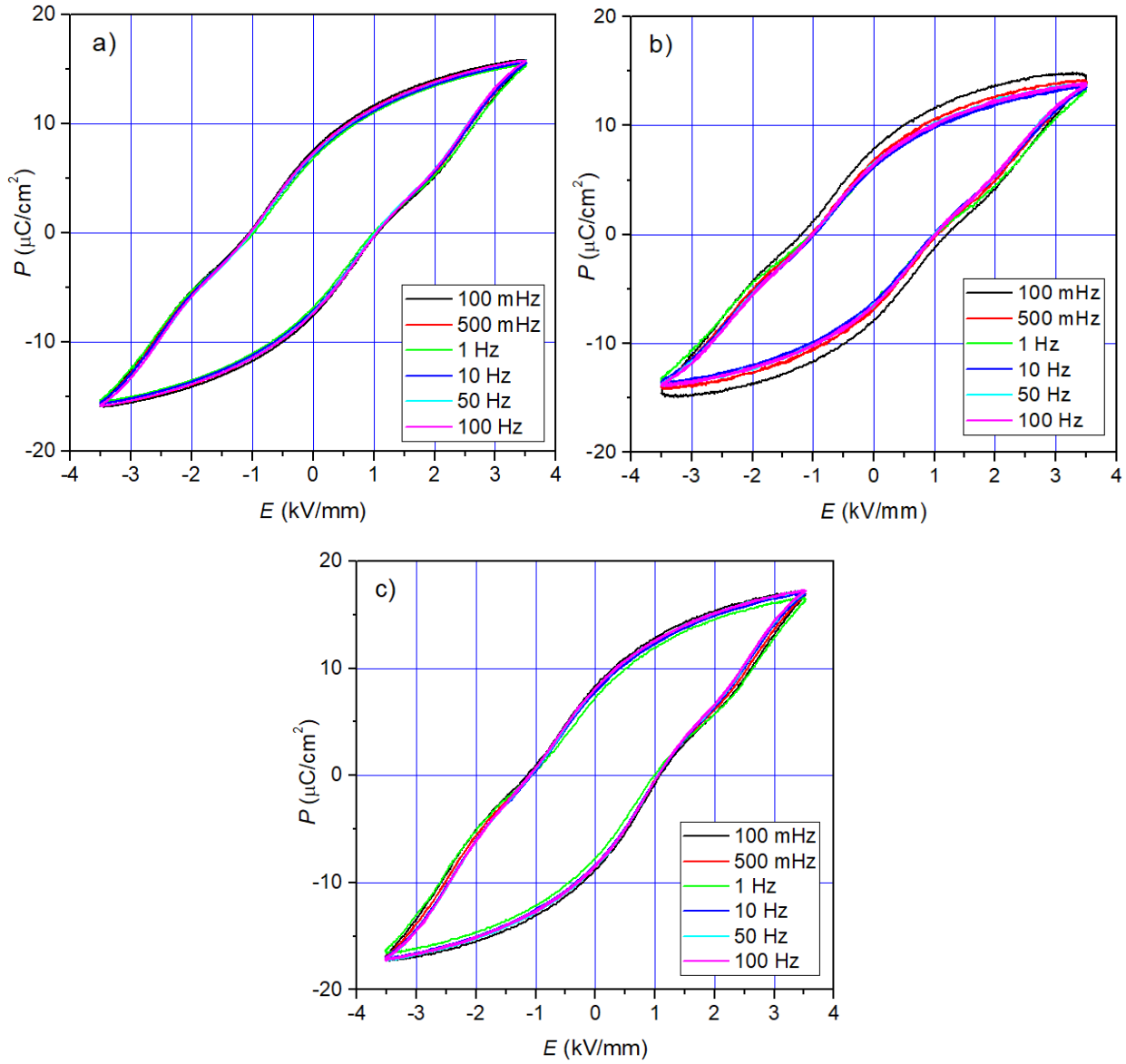


Fig. 10. Hysteresis *P-E* loops for unpolarized PZT-type ceramic samples (100 mHz-100 Hz, *RT*): a) s-La12, b) s-La10, c) s-La08

dipole moments in each unit cell. Ferroelectric properties tests (*P-E* hysteresis loop test) of the unpolarized PZT ceramics were carried out at room temperature, for the frequency of the measuring field from 100 mHz to 100 Hz and at the field intensity of 3.5 kV/mm (Fig. 10).

For all samples the hysteresis loops are linear type (with a large coercive field), characteristic for perovskite type materials with tetragonal structure. The *P-E* studies showed high values of spontaneous polarization ($P_s$) as well as residual polarization ($P_r$) of the samples. Increasing the frequency of the measurement field reduces the coercivity field. For all samples the hysteresis loops show characteristic necking. An extreme case of this phenomenon is a characteristic double hysteresis loop characterized by materials with antiferroelectric properties.

The results of *P-E* hysteresis loop for all samples, for 1 Hz, depicted in Fig. 11. The graphs present cyclic application to samples of an increasingly higher the field intensity in the range from 0.5 kV/mm to 3.5 kV/mm. $E_C$ coercive field values are: 0.915 kV/mm, 1.01 kV/mm and 0.967 kV/mm for the s-La12, s-La10 i s-La08 samples, respectively. For a ceramic materials the coercive field provides an specify of grain size. Ceramic samples with low values of $E_c$ have microstructure with large grains, while a high $E_c$ implies small grain. Higher values of $E_c$ for s-La12 sample was attributed to the difficulty of domain polarization reversal in the smaller grains. The lower values of $E_c$ have an advantage in device applications since the power losses are minimized and the switching voltage reduced [39].

The tests showed slight differences in the residual polarization values and the coercive field with the change in the amount of lanthanum in the base composition.

Ferroelectric materials above the phase transition temperature will lose the ferroelectric state and the $P_s$ spontaneous polarization. Therefore, the working temperature of microelectronic devices made of ferroelectric materials is limited by the Curie temperature ($T_C$) and in practice is limited to one-half of the $T_C$ due to the loss of polarization [40].

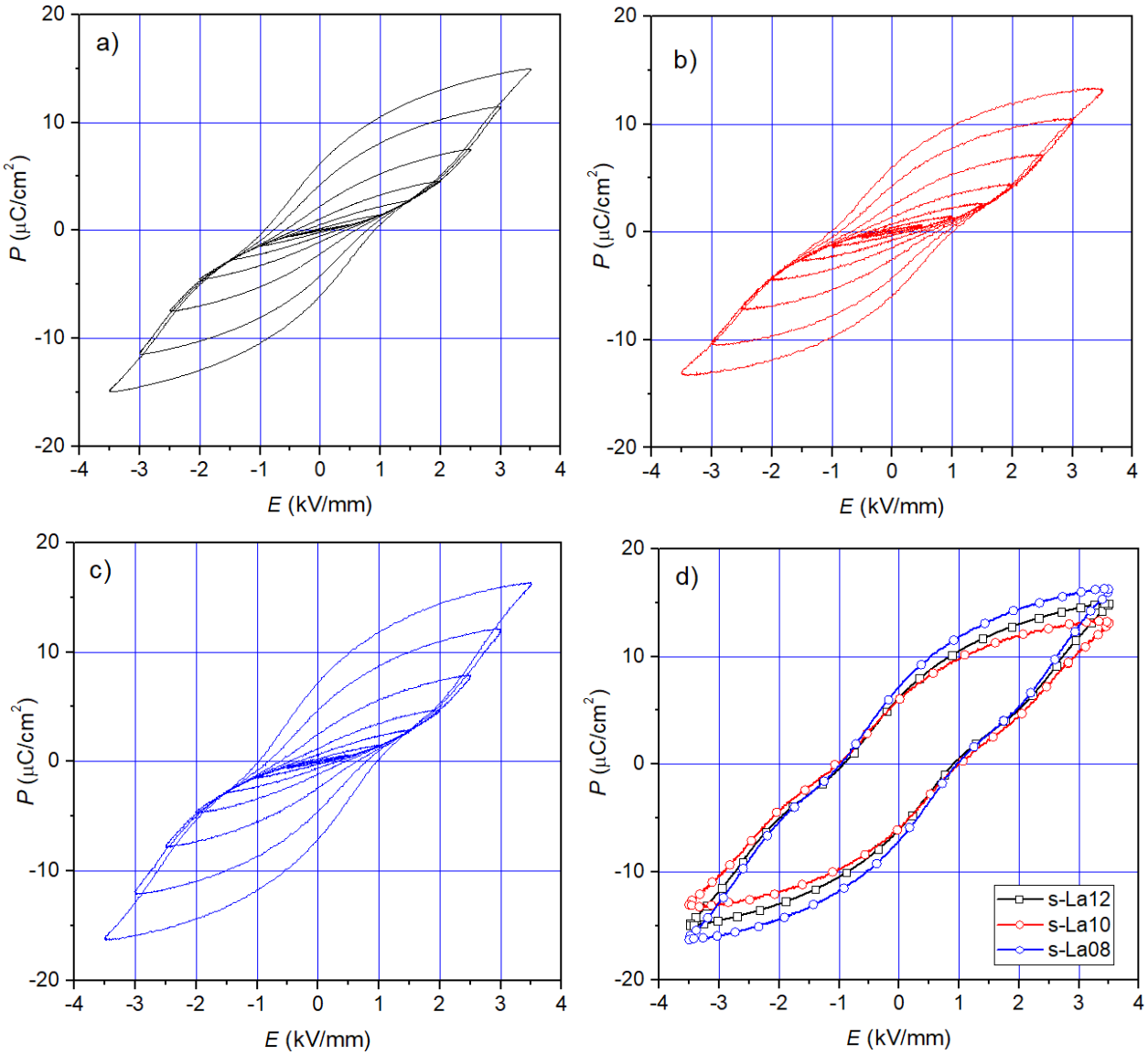


Fig. 11. The hysteresis loops at room temperature for the unpolarized PZT-type ceramics at various electric fields (a-c) and (d) summary *P-E* tests for all samples (1 Hz)

The PZT-type ceramic samples were polarized in silicone oil by the high-voltage method. The parameters calculated according to the resonance-antiresonance method, are presented in Table 1. The PZT-type ceramic samples shows good values of the piezoelectric parameters, which predisposes the multicomponent material to micromechatronic applications (e.g., as an element in actuators, piezoelectric transducers, etc.). The values of piezoelectric coefficient $d_{33}$ measured at room temperature of the PZT-type ceramic samples are included in the range from 324 pC/N to 336 pC/N.

In comparison with the undoped PZT ceramics, the obtained doped ceramic materials show higher values of electrical permittivity, high electrical resistivity and low coercive field. Ceramic elements show high sensitivity to external electric fields (easy polarization / depolarization). This kind of doping (donor-doped) is used when designing soft PZT-type materials. The good electric and piezoelectric properties of the multi-component ceramics, allowed using this type materials as an element to build actuators, sensors and transducers. The high value of dielectric permittivity of ceramic materials increases the capacity of conductor systems, which is also used in the construction of capacitors.

## 4. Conclusion

In the paper three PZT-type ceramics doped by $Mn^{4+}$, $Sb^{3+}$, $La^{3+}$, $W^{6+}$ have been designed and obtained by classical technology.

The X-ray tests confirmed that designed and obtained materials belong to perovskite type structure of the tetragonal crystallographic system. Studies have also shown that all samples exhibit single-phase (no foreign, undesirable phase and no other impurities). The microstructures of the ceramic samples prove that the technological process has been properly carried out and correctly selected technological conditions (ceramic grains exhibit a correct angular shape). All obtained compositions

show high values of dielectric permittivity with a sharp ferroelectic-paraelectric phase transition as well as very low value of dielectric loss. A slight change in the amount of lanthanum (in the range from 0.008 to 0.012) at the expense of the amount of tungsten (in the range from 0.012 to 0.014) does not change the nature of the electrical conductivity in the ceramic samples.

The good electric and piezoelectric properties of the PZT-type ceramics, allowed using this type materials as an element to build actuators, sensors and transducers in modern micromechatronic and microelectronic devices.

## REFERENCES

[1] Z.-G. Ye, Handbook of Advanced Dielectric, Piezoelectric and Ferroelectric Materials. Synthesis, Properties and Applications; Woodhead Publishing: Cambridge, England 2008.

[2] A.J. Moulson, J.M. Herbert, Electroceramics: Materials, Properties, Applications; second ed., Wiley, Chichester, West Sussex, 2003.

[3] X. Li, J.S. Vartuli, D.L. Milius, I.A. Aksay, W.Y. Shih, W.-H. Shih, J. Am. Ceram. Soc. **84**, 996-1003 (2001).

[4] P.-H. Xiang, X.-L. Dong, H. Chen, Z. Zhang, J.-K. Guo, Ceram. Int. **29**, 499-503 (2003).

[5] H. Wei, Y. Chen, Ceram. Int. **41**, 6158-6163 (2015).

[6] N. Texier, Ch. Courtois, M. Traianidis, A. Leriche, J. Eur. Ceram. Soc. **21**, 1499-1502 (2001).

[7] B. Jaffe, R. Cook, H. Jaffe, Piezoelectric Ceramics. Academic Press, New York, 1971: 135

[8] A.S. Karapuzha, N.K. James, H. Khanbareh, S. van der Zwaag, W.A. Groen, Ferroelectrics **504**, 160-171 (2016).

[9] E. Boucher, B. Guiffard, L. Lebrun, D. Guyomar, Ceram. Int. **32**, 479-485 (2006).

[10] M.V. Ramanaa, S.R. Kiran, N.R. Reddy, K.V.S. Kumar, V.R.K. Murthy, B.S. Murty, Mater. Chem. Phys. **126**, 295-300 (2011).

[11] W. Qiu, H.H. Hng, Mater. Chem. Phys. **75**, 151-156 (2002).

[12] R. Zachariasz, D. Bochenek, K. Dziadosz, J. Dudek, J. Ilczuk, Arch. Metall. Mater. **56**, 1217-1222 (2011).

[13] J. Li, Q. Sun, Rare Metals **27**, 362-366 (2008).

[14] D. Bochenek, P. Niemiec, R. Zachariasz, A. Chrobak, G. Ziółkowski, Arch. Metall. Mater. **58**, 1013-1017 (2013).

[15] P. Niemiec, D. Bochenek, A. Chrobak, P. Guzdek, A. Błachowski, Int. J. Appl. Ceram. Tec. **12**, E82-E89 (2015).

[16] R. Zachariasz, J.A. Bartkowska, D. Bochenek, P. Niemiec, Arch. Metall. Mater. **58**, 1327-1330 (2013)

[17] D. Bochenek, P. Niemiec, J. Korzekwa, B. Durtka, Z. Stokłosa, Symmetry **10**, 59, (2018).

[18] R. Zachariasz, D. Bochenek, P. Niemiec, J. Ilczuk, J.A. Bartkowska, D. Brzezińska, Mech. Syst. Signal Pr. **78**, 84-90 (2016).

[19] C.-W. Nan, L. Liu, N. Cai, J. Zhai, Y. Ye, Y.H. Lin, L.J. Dong, C.X. Xiong, Appl. Phys. Lett. **81**, 3831 (2002).

[20] J. Yao, Ch. Xiong, L. Dong, Ch. Chen, Y. Lei, L. Chen, R. Li, Q. Zhu, X. Liu, J. Chem. Mater. **19**, 2817-2821 (2009).

[21] N. Izyumskaya, Y.I. Alivov, S.J. Cho, H. Morkoç, H. Lee, Y.S. Kang, Critical Reviews in Solid State and Materials Sciences **32**, 111-202 (2007).

[22] Z. Hu, R.C. Smith, J. Ernstberger, J. Intel. Mat. Syst. Str. **23**, 1869-1894 (2012).

[23] O. Bilgen, C. Jr. De Marqui, K.B. Kochersberger, D.J. Inman, J. Intel. Mat. Syst. Str. **22**, 81-91 (2011).

[24] J. Nuffer, T. Bein, Applications of piezoelectric materials in the transportation industry. Global Symposium on Innovative Solutions for the Advancement of the Transport Industry. San Sebastian, Spain, 2006.

[25] Y. Shi, S.R. Hallett, M. Zhu, Compos. Struct. **160**, 1279-1286 (2017).

[26] V. Kumar, M. Hays, E. Fernandez, W. Oates, F.S. Alvi, Smart Materials and Structures 20, 105033 (2011).

[27] D.J. Leo, Engineering Analysis of Smart Material Systems, John Wiley and Sons, Inc., Hoboken, NJ, 2007.

[28] R.C. Smith, Smart Material Systems: Model Development, SIAM, Philadelphia, PA, 2005.

[29] K. Uchino, Ferroelectric Devices; 2nd Edition, CRC Press/Taylor and Francis, Boca Raton, FL, 2010.

[30] K. Uchino, J.R. Giniewicz, Micromechatronics, Marcel Dekker, Inc., New York, 2003.

[31] D. Vasic, E. Sarraute, F. Costa, P. Sangouard, E. Cattan, J. Micromech. Microeng. **14**, S90-S96. (2004).

[32] M. Morawiec, A. Grajcar, Journal of Achievements in Materials and Manufacturing Engineering **80**, 11-17 (2017).

[33] T. Yu, Z.X. Shen, W.S. Toh, J.M. Xue, J. Wang, J. Appl. Phys. **94**, 618-620 (2003).

[34] G. Williamson, R. Smallman, Philos. Mag. **1**, 34-46 (1956).

[35] A. Gantassi, H. Essaidi, K. Boubaker, J.C. Bernède, A. Colantoni, M. Amlouk, T. Manoubi, Mat. Sci. Semicon. Proc. **24**, 237-248 (2014).

[36] Q.M. Zhang, H. Wang, N. Kim, L.E. Cross, J. Appl. Phys. **75**, 454-459 (1994).

[37] D. Bochenek, Z. Surowiak, J. Krok-Kowalski, J. Poltierova-Vejpravova, J. Electroceram. **25**, 122-129 (2010).

[38] T. Frömling, A. Schintlmeister, H. Hutter, J. Fleig, J. Am. Ceram. Soc. **94**, 1173-1181 (2011).

[39] P. Kou, S.K. Sinha, Dig. J. Nanomater. Bios. **7**, 3, 1327-1332 (2012).

[40] J. Chen, X. Tan, W. Jo, J. Rodel, J. Appl. Phys. **106**, 034109 (2009).